Anisotropic supercurrent suppression and revivals in a graphene-based Josephson junction under in-plane magnetic fields

Philipp Schmidt [1,2,*] Katarina Stanojević [1,*] Kenji Watanabe [3] Takashi Taniguchi [4] Bernd Beschoten [1] Vincent Mourik [5] and Christoph Stampfer [1,2,†]

[1]*JARA-FIT and 2nd Institute of Physics, RWTH Aachen University, 52074 Aachen, Germany*

[2]*Peter Grünberg Institute (PGI-9), Forschungszentrum Jülich GmbH, 52425 Jülich, Germany*

[3]*Research Center for Electronic and Optical Materials, National Institute for Materials Science, 1-1 Namiki, Tsukuba 305-0044, Japan*

[4]*International Center for Materials Nanoarchitectonics, National Institute for Materials Science, 1-1 Namiki, Tsukuba 305-0044, Japan*

[5]*JARA Institute for Quantum Information (PGI-11), Forschungszentrum Jülich GmbH, 52425 Jülich, Germany*

(Received 1 February 2025; revised 28 April 2025; accepted 16 May 2025; published 6 June 2025)

We report on a tunable Josephson junction formed by a bilayer graphene ribbon encapsulated in WSe_2 with superconducting niobium contacts. We characterize the junction by measurements of the magnetic field–induced interference pattern and the AC Josephson effect manifested as Shapiro steps, examining current-dependent hysteresis and junction dynamics. The latter can be tuned by temperature, gate voltage, and magnetic field. Finally, we examine the evolution of the supercurrent when subjected to in-plane magnetic fields. Notably, we observe strong anisotropy in the supercurrent with respect to the orientation of the in-plane magnetic field. When the field is parallel to the current direction, the supercurrent is suppressed and shows revivals with increasing magnetic field, whereas it remains almost unaffected when the field is oriented in a perpendicular direction. We suggest that this anisotropy is caused by the dependence of supercurrent interference on the junction geometry.

DOI: 10.1103/PhysRevB.111.245301

I. INTRODUCTION

Josephson junctions exploit the quantum mechanical phenomenon where a supercurrent flows between two superconductors separated by a thin insulating or normal conducting weak link [1–5]. The unique properties of graphene provide a tunable weak link with highly transparent interfaces due to absence of Schottky barriers [6,7], while the high carrier mobility of graphene, enabling ballistic transport [8,9], together with its ability to host proximity-induced superconductivity, make it an attractive candidate for next-generation Josephson junctions [10,11]. Graphene Josephson junctions offer several advantages over conventional junctions. Their tunability via electrostatic gating allows for dynamic control of junction properties, potentially leading to tailored and reconfigurable quantum devices [12–15]. Additionally, the implementation of a high spin-orbit material such as WSe_2, that gets proximity-coupled to a bilayer graphene, allows us to implement Josephson junctions that potentially host topologically protected states [16], which are of importance for the ongoing search for non-Abelian phases of matter [17–20].

In recent years, graphene-based Josephson junctions have been intensively investigated [7,21–43]. So far, the influence of a magnetic field applied in the plane of the Josephson junction has not been systematically and angle-resolved investigated. However, tuning the Zeeman energy in these Josephson junctions by an in-plane magnetic field is crucial for the formation of topologically protected states [16,44–46].

In this paper, we report on a study of a tunable graphene-based Josephson junction formed by a bilayer graphene ribbon encapsulated in WSe_2 with superconducting niobium (Nb) contacts. We present a detailed characterization of the junction, which includes magnetic interference as well as Shapiro step measurements where we examine the difference between the switching currents and the damping behavior. Furthermore, we investigate the evolution of the supercurrent when the junction is subject to in-plane magnetic fields. A strong anisotropy of the supercurrent is observed with respect to the orientation of the in-plane magnetic field, and we suggest that in-plane geometric interference effects may be its origin.

II. SAMPLE LAYOUT AND BASIC TRANSPORT CHARACTERISTICS

A schematic and an atomic force micrograph of our device are shown in Figs. 1(a) and 1(b), respectively. The device consists of a bilayer graphene flake symmetrically encapsulated in single layers of WSe_2 and thicker flakes of hexagonal boron nitride (hBN) using automated flake search [47] and dry transfer stacking [8]. The stack is etched into a $w = 2.1\,\mu$m-wide ribbon by SF_6/O_2 reactive ion etching (RIE) through a polymethyl methacrylate resist mask, which has been patterned

*These authors contributed equally to this work.
†Contact author: stampfer@physik.rwth-aachen.de

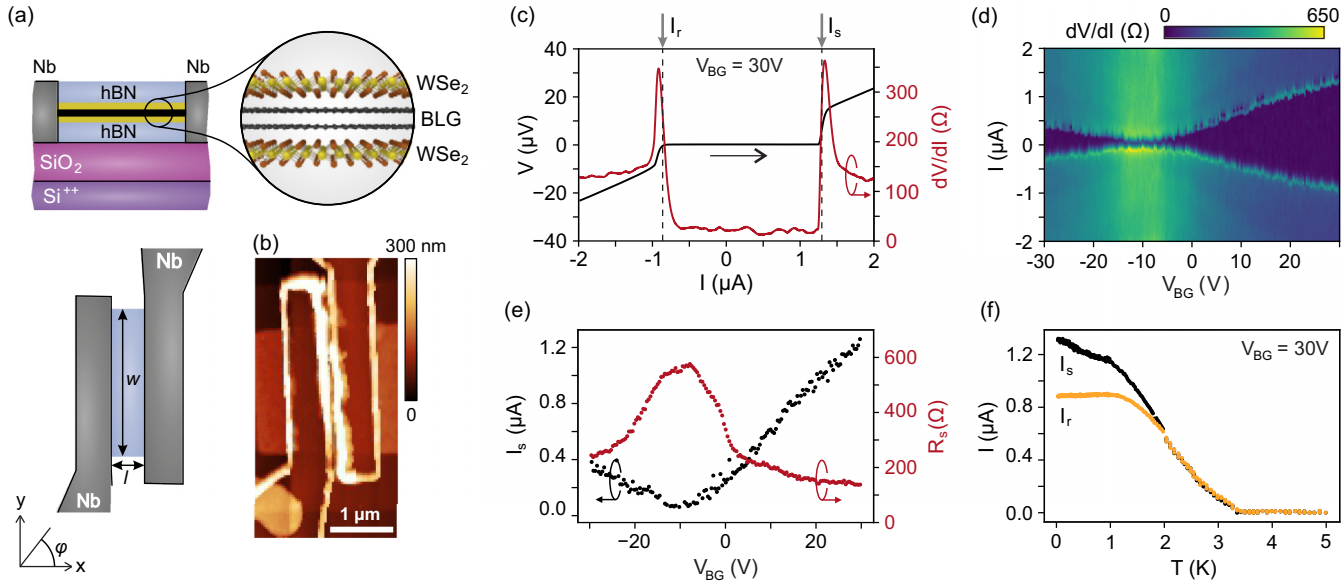

FIG. 1. (a) Schematic of the Josephson junction. Side and top views of the device with a length of 250 nm and a width of 2.1 µm is shown. The bilayer graphene (BLG) is located between two flakes of WSe_2, encapsulated in hBN and contacted by superconducting niobium (Nb) contacts. The van der Waals heterostructure is placed onto a Si^{++}/SiO_2 back gate. (b) Scanning force microscope image of the examined device showing the etched ribbon and the two niobium contacts. (c) DC voltage and differential resistance dV/dI as a function of bias current at $V_{BG} = 30$ V. The bias current was swept from negative to positive values. (d) Differential resistance as a function of applied back gate voltage and bias current. (e) Extracted switching current I_s and resistance R_s as function of back gate voltage. (f) Temperature-dependent switching current I_s and retrapping current I_r at $V_{BG} = 30$ V.

by standard electron beam lithography. The bilayer graphene is electrically contacted to 25-nm-thick superconducting Nb electrodes, fabricated by RIE and consecutive sputter deposition through the same resist mask without any cleaning steps in between. This defines the junction length of $l = 0.25\,\mu$m. The device is placed on a highly doped silicon substrate serving as a back gate, with a 285-nm-thick separating SiO_2 gate dielectric. This allows us to adjust the charge carrier density of the bilayer graphene to $n = \alpha(V_{BG} - V_{BG}^0)$, where α_{BG} represents the gate lever arm, which is proportional to the capacitive coupling between the back gate and the bilayer graphene. For more details on the fabrication procedure and a characterization of the Nb film, see Secs. S1 and S2 in the Supplemental Material [48].

All measurements were conducted in a He^3/He^4 dilution refrigerator at a base temperature of 30 mK, using a four-terminal low-frequency lock-in technique with an applied current bias, see Sec. S3 in the Supplemental Material [48]. In Fig. 1(c), we show a representative *V-I* curve as well as the differential resistance of the Josephson junction at a back gate voltage of $V_{BG} = 30$ V. Here, the bias current is swept from negative to positive values. The switching current I_s can be identified as the switching from the superconducting to the resistive state at positive bias current, while the switching from the resistive to the superconducting state at negative bias currents defines the retrapping current I_r. In Fig. 1(d), the differential resistance dV/dI of the device is shown as a function of the bias current I and back gate voltage V_{BG}. The superconducting regime (visible as the dark blue region) appears around $I = 0$ for both electron doping ($V_{BG} > -8$ V) and hole doping ($V_{BG} < -8$ V), clearly distinct from the resistive regime at higher bias current values. The extracted gate voltage–dependent switching current I_s and switching resistance R_s are shown in Fig. 1(e). The I_sR_s product of the junction ranges from 40 to 180 µV, see Sec. S6 in the Supplemental Material [48]. Furthermore, we show the temperature dependence of I_s and I_r at $V_{BG} = 30$ V, see Fig. 1(f). The temperature-dependent difference between I_s and I_r, which emerges <2 K, can be understood by evaluating the quality factor of the junction $Q = \sqrt{2eI_sR_s^2C/\hbar}$ in the framework of the resistively and capacitively shunted junction (RCSJ) model that describes the dynamics of a Josephson junction by considering it as a parallel combination of a resistor, capacitor, and an ideal Josephson element [49,50]. Here, the junction capacitance, estimated by fitting the RCSJ model to a measured *V-I* curve (see Sec. S5 in the Supplemental Material [48] for details), is $C = 0.1$ pF, and by measuring I_s, the quality factor is determined, which changes from $Q > 1$ to $Q < 1$ at a temperature of 2.5 K. Therefore, the junction dynamics changes from the underdamped to the overdamped regime where I_s and I_r become equal. Further details on the damping and quality factor are presented in Sec. S7 in the Supplemental Material [48].

III. SHAPIRO STEPS

To study the junction dynamics in more detail, we investigate the influence of microwave radiation on the *V-I* curve of the junction. Applying microwave radiation leads to the AC Josephson effect, which is manifested in additional plateaus in the DC voltage [51], known as Shapiro steps. These steps occur at integer multiples of $hf/2e$ and result from the phase

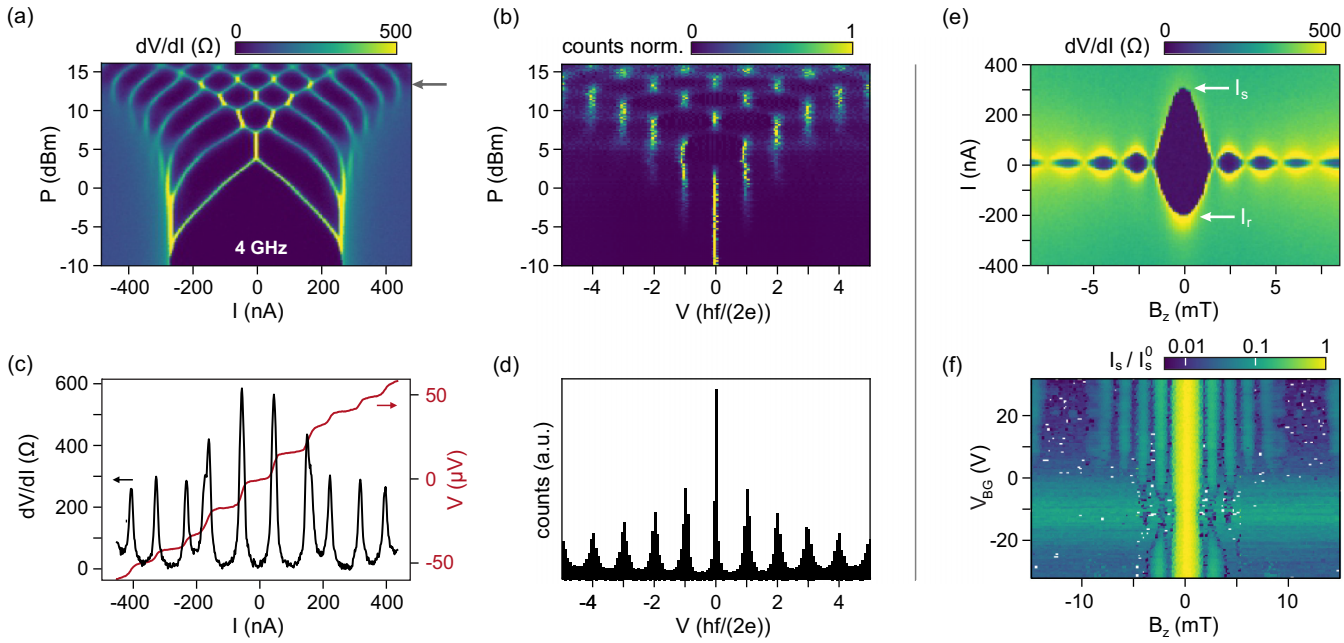

FIG. 2. (a) Differential resistance as a function of RF signal power and bias current measured at a drive frequency of 4 GHz and a back gate voltage of $V_{BG} = 30$ V. A magnetic field of $B_z = 1.25$ mT was used to decrease the switching current. (b) Normalized histogram of the DC voltages in units of $hf/(2e)$ as a function of RF signal power. More Shapiro steps emerge with increasing power. (c) DC voltage (red) and differential resistance (black) as a function of bias current at an RF power of 13.8 dBm. (d) The sum of the histogram with pronounced peaks at integer values of V_{dc} in units of $hf/(2e)$. (e) Differential resistance as a function of perpendicular magnetic field B_z and bias current for $V_{BG} = 0$ V. (f) Extracted normalized switching current as a function of B_z and back gate voltage V_{BG}.

locking across the junction to the external frequency. Here, h is the Planck constant, f the frequency of the radio frequency (RF) signal source, and e the elementary charge. The formation of Shapiro plateaus with increasing microwave power is visible in Fig. 2(a), where the measurement was taken at $V_{BG} = 30\,V$ and $f = 4\,\text{GHz}$. Here, the differential resistance is shown as a function of applied bias current I and the applied signal power. The pattern qualitatively resembles the expectation for weakly damped Josephson junctions where the extension of the steps surpass I_s and superconducting pockets develop in the normal conducting region. We also observe broad regions of microwave power where the resistive transition is an extended line instead of single points expected for the Bessel function behavior of overdamped Josephson junctions [52]. This behavior has also been observed in other graphene Josephson junctions [53–55] and may be explained by the junction being underdamped and having a high plasma frequency. The first Shapiro plateau starts to develop at −7 dBm, whereas at higher powers, many different plateaus emerge separated by sharp peaks in the dV/dI curve, as depicted in Fig. 2(c). Moreover, the quantization of these steps can be seen in the power-dependent histogram of the DC voltages in Fig. 2(b), where the steps emerge at integer multiples of $hf/2e$. This is also reflected in sharp peaks of the sum histogram, see Fig. 2(d). All integer Shapiro steps are present without any subinteger steps appearing, unlike what is observed in other two-dimensional Josephson junctions [56,57], suggesting that the current phase relationship is not strongly skewed. Additional Shapiro step measurements are shown in Sec. S8 in the Supplemental Material [48].

IV. SUPERCURRENT INTERFERENCE

Next, we examine the magnetic field dependence of the switching current for both out-of-plane and in-plane directions. We start with out-of-plane magnetic fields and measure the differential resistance vs both the current I and the out-of-plane magnetic field B_z. The phase difference between the two superconductors induced by the magnetic field leads to a modulation of the switching current I_s [58], as illustrated in Fig. 2(e). Analyzing the periodicity of the modulation pattern leads to an effective junction length of 603 nm and a magnetic penetration depth of $\lambda \approx 175\,\text{nm}$, with the area of the weak link determined from atomic force microscopy measurements, see Sec. S4 in the Supplemental Material [48] for details. The resulting penetration depth is in reasonable agreement with $\lambda_{Nb} = 150\,\text{nm}$ reported for niobium [59]. We note that the oscillation period of the supercurrent modulation pattern remains unchanged irrespective of the applied gate voltage, see Fig. 2(f). This is in contrast with previous work on BLG/WSe_2, where a $2\Phi_0$ signature has been observed in the interference pattern at charge neutrality [43].

In Fig. 2(e), a pronounced difference between the switching current and the retrapping current can be seen around the central lobe. This behavior can again be explained by a tunable quality factor Q as the magnetic field–induced modulation of the switching current leads to a transition of the quality factor from $Q \approx 3$ at the central lobe to $Q \approx 1$ at higher lobes, accompanied by a transition from the underdamped to the hysteresis-free junction dynamics.

We now analyze the behavior of the junction for an in-plane magnetic field ($B_{||}$) varying the angle (φ), which is defined in

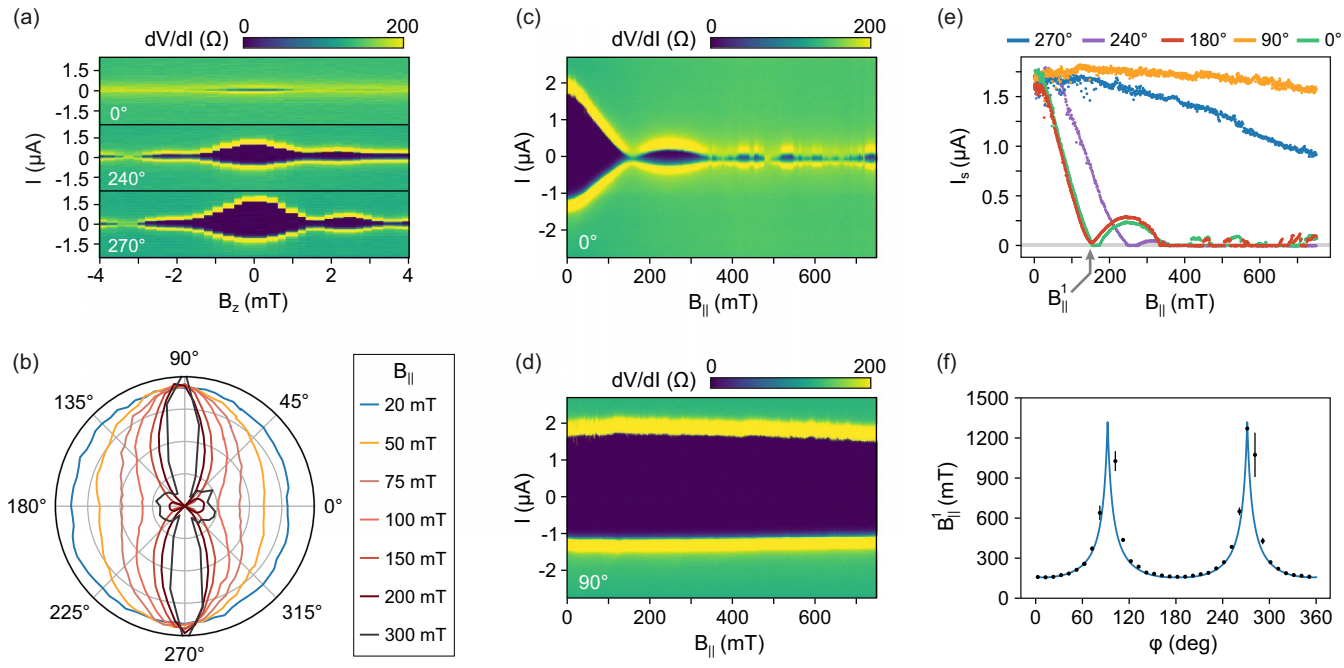

FIG. 3. (a) Differential resistance as function of current and out-of-plane magnetic field for $B_{||} = 150$ mT at in-plane angles $\varphi = 0°$, 240°, and 270°. (b) Polar representation of the maximum of I_s, extracted from the interference measurements, as a function of φ for varying $B_{||}$. (c) and (d) Differential resistance as function of current and $B_{||}$ applied in the direction of the current ($\varphi = 0°$) and perpendicular $\varphi = 90°$. (e) Extracted switching current as a function of $B_{||}$ for various in-plane angles φ. The gray bar indicates the region of nondetectable switching current. (f) In-plane magnetic field of the first supercurrent minimum $B_{||}^1$ for different angles φ. Solid gray line represents a fit to the geometrical model described in the text. An outlying point at 90° at ∼3 T is not included. See Sec. S10 in the Supplemental Material [48] for the extraction (for minima up to 300 mT) or extrapolation procedure (for minima beyond 300 mT).

Fig. 1(a). First, the B_z-induced interference pattern is shown in Fig. 3(a) at $B_{||} = 150$ mT applied at different angles. When the in-plane magnetic field is oriented parallel to the direction of the current ($\varphi = 0°$ and 180°), the supercurrent is most strongly suppressed [see upper panel in Fig. 3(a)]. However, it reappears at skewed angles, such as 240°, and reaches a maximum when the field is perpendicular to the current ($\varphi = 270°$). This behavior is summarized in a polar plot of the maximum switching current plotted as a function of the in-plane angles and the amplitude of $B_{||}$ in Fig. 3(b). With increasing amplitude of $B_{||}$, the supercurrent shows increased anisotropy. While I_s is largely unaffected when $B_{||}$ is oriented perpendicular to the current direction at $\varphi = 90°$ and 270°, it is suppressed when the field is parallel to it. It becomes zero near $B_{||} = 150$ mT and even reappears at larger field amplitudes. Additional data on the evolution of the interference pattern subject to in-plane magnetic fields are presented in Sec. S9 in the Supplemental Material [48].

Sweeping $B_{||}$ for different in-plane angles, as shown in Fig. 3(c), reveals not only significant anisotropy in the switching current but also supercurrent revival effects depending on the orientation of the magnetic field. This is in stark contrast with the configuration where the magnetic field is oriented perpendicular to the current direction for $\varphi = 270°$ [see Fig. 3(d)], where the supercurrent only decreases by ∼200 nA over the entire range of the magnetic field. This anisotropy is further illustrated in Fig. 3(e) by showing the extracted maximum supercurrent for various angles. For angles perpendicular to the supercurrent flow direction, a monotonous decrease of ≈15% throughout the investigated field range is observed, while tilting the in-plane magnetic field toward the supercurrent flow direction leads to a progressively stronger suppression of the supercurrent, with the field of the first minimum eventually reaching the smallest value of 150 mT.

To further analyze this anisotropy, we extract the in-plane magnetic field value $B_{||}^1$, corresponding to the first minimum of I_s (see Sec. S10 in the Supplemental Material [48] for a discussion and details) and plot it as a function of φ, see Fig. 3(f). Assuming a finite effective thickness of the junction d_{eff}, the in-plane magnetic field induces a magnetic flux $\Phi_{||} = B_{||} d_{\text{eff}} [|w \cos(\varphi)| + |l \sin(\varphi)|]$. In case supercurrent suppression and its anisotropy are caused by interference effects, the first supercurrent minimum appears at magnetic fields of order $B_{||}^1 = \Phi_0 / \{d_{\text{eff}} [|w \cos(\varphi)| + |l \sin(\varphi)|]\}$. A fit of this model to the extracted data results in an effective thickness of $d_{\text{eff}} = 6.3$ nm.

Supercurrent interference under in-plane magnetic fields can be understood in a qualitative microscopic picture. In a perfectly homogeneous two-dimensional Josephson junction, supercurrent is carried by identical Andreev bound states (ABSs) in many identical parallel transport channels. Here, magnetic flux is threaded through the out-of-plane orbital component of the ABS wave function for any in-plane angle φ (in principle allowing for interference for any value of φ), but due to the identical orbital wave functions, no interference occurs. However, such an idealized picture is not

realistic, as it ignores microscopic disorder that will cause the many ABSs present to have, at best, similar but not identical orbital wave functions. This will lead to the buildup of phase differences between the individual ABSs under in-plane magnetic field, and the total supercurrent integrated over the entire junction will display an averaged orbital interference effect.

Possible disorder mechanisms in our devices are residual geometric disorder after encapsulating bilayer graphene between WSe_2 and hBN and electrostatic disorder, for example, due to defects and contaminants at the various interfaces in the layer stack [60,61]. Additionally, a narrow section of the junction in the contact area may be more strongly disordered, which may enhance supercurrent interference effects.

Beyond disorder-enabling supercurrent interference effects, the assumption of a homogeneous in-plane magnetic field is not realistic. Flux focusing effects caused by the presence of superconducting contacts may allow for small out-of-plane components of the magnetic field, which are expected to be highly dependent on the exact device geometry. In an earlier work [62], the anisotropy of in-plane supercurrent interference was fully attributed to flux focusing. Further texture may be added to the magnetic field by irregularities in the shape of the superconducting contacts and the possibility of vortices also entering the niobium film under in-plane magnetic fields.

Our experiment cannot discriminate between the possible causes of supercurrent interference. Assuming such effects are significant, we expect supercurrent interference for any value of φ and a geometric dependence on φ, rationalizing our phenomenological fitting procedure. We conjecture that d_{eff} introduced above is a phenomenological parameter that absorbs microscopic disorder effects, flux focusing, and other magnetic field inhomogeneities into a single fitting parameter. Its value of 6.3 nm is about an order of magnitude larger than the thickness of the bilayer graphene, which means that the effective transverse area of the junction through which flux can be threaded is enlarged by the various possible causes of supercurrent interference.

Relating d_{eff} to a microscopic model and assessing its value, while disentangling the effect of flux focusing, requires modeling efforts beyond the scope of this paper. Such modeling could rely on introducing a randomization of the junction geometry in an otherwise standard classical approach following [52]. Alternatively, a quantum mechanical electronic transport approach could be followed, extending such modeling carried out for quasi-one-dimensional nanowire-based Josephson junctions [63] to two-dimensional Josephson junctions. Any such modeling should be approached with caution due to risks of overfitting the data by introducing additional modeling parameters when attempting to create more realistic models.

Alternative mechanisms predicting decay and revival of supercurrent under in-plane magnetic fields rely on spin physics stemming from the semiconducting band structure incorporated into the effective Hamiltonian of the Josephson junction. Such proposed effects include 0π transitions of the ground state of the junction due to the Zeeman effect [64,65], similar transitions but to arbitrary phase differences ϕ_0 (so-called ϕ_0 junctions) [66,67] due to additional spin-orbit interaction, or more exotic physics such as topological phase transitions. However, for significant spin splitting to occur, which is a prerequisite for such effects, much larger magnetic fields of the order of several Teslas are anticipated in bilayer graphene. We observe supercurrent minima already at values as low as 150 mT, rendering spin-physics-related explanations implausible.

V. CONCLUSION

In summary, we have presented a tunable lateral Josephson junction consisting of bilayer graphene encapsulated in WSe_2. We have been able to tune the junction quality factor and thus its damping regime by external parameters, such as back gate voltage, magnetic field, and temperature. This is evident from the magnetic field–induced modulation of the switching current and the retrapping current. Furthermore, we see well-defined Shapiro steps under RF driving of the junction. We observe a highly anisotropic suppression and revival of the supercurrent when the Josephson junction is subject to in-plane magnetic fields. We suspect that this anisotropic behavior is caused by orbital interference of the supercurrent. Further research on quasi two-dimensional Josephson junctions at finite in-plane magnetic fields is required to obtain an in-depth understanding in these systems. We caution against narratives that fail to consider interference effects when invoking supercurrent suppression and revival to support claims of observing spin phenomena originating from the semiconducting band structure.

ACKNOWLEDGMENTS

We thank L. Banszerus, S. Anupam, and S. M. Frolov for insightful discussions. This project has received funding from the Deutsche Forschungsgemeinschaft under Germany's Excellence Strategy—Cluster of Excellence Matter and Light for Quantum Computing EXC 2004/1—390534769, from the European Research Council under the European Union's Horizon 2020 research and innovation programme (Grant Agreement No. 820254), and the Helmholtz Nano Facility [68]. K.W. and T.T. acknowledge support from the JSPS KAKENHI (Grants No. 21H05233 and No. 23H02052) and World Premier International Research Center Initiative, MEXT, Japan.

P.S., V.M., and C.S. conceived this experiment. P.S. and K.S. fabricated the device, performed the measurements, and analyzed the data. P.S. performed the simulation. K.W. and T.T. synthesized the hBN crystals. B.B., V.M., and C.S. supervised the project. P.S., K.S., and V.M. wrote the manuscript with contributions from all authors. P.S. and K.S. contributed equally.

DATA AVAILABILITY

The data that support the findings in this paper are openly available [69].

[1] B. D. Josephson, Possible new effects in superconductive tunnelling, Phys. Lett. **1**, 251 (1962).

[2] P. G. de Gennes, Boundary effects in superconductors, Rev. Mod. Phys. **36**, 225 (1964).

[3] P. W. Anderson and J. M. Rowell, Probable observation of the Josephson superconducting tunneling effect, Phys. Rev. Lett. **10**, 230 (1963).

[4] C. John, Supercurrents in lead–copper–lead sandwiches, Proc. R. Soc. Lond. A **308**, 447 (1969).

[5] J. G. Shepherd, Supercurrents through thick, clean S–N–S sandwiches, Proc. R. Soc. London A **326**, 421 (1972).

[6] G. Giovannetti, P. A. Khomyakov, G. Brocks, V. M. Karpan, J. van den Brink, and P. J. Kelly, Doping graphene with metal contacts, Phys. Rev. Lett. **101**, 026803 (2008).

[7] H. B. Heersche, P. Jarillo-Herrero, J. B. Oostinga, L. M. K. Vandersypen, and A. F. Morpurgo, Bipolar supercurrent in graphene, Nature (London) **446**, 56 (2007).

[8] L. Wang, I. Meric, P. Y. Huang, Q. Gao, Y. Gao, H. Tran, T. Taniguchi, K. Watanabe, L. M. Campos, D. A. Muller *et al.*, One-dimensional electrical contact to a two-dimensional material, Science **342**, 614 (2013).

[9] L. Banszerus, M. Schmitz, S. Engels, M. Goldsche, K. Watanabe, T. Taniguchi, B. Beschoten, and C. Stampfer, Ballistic transport exceeding 28 μm in CVD grown graphene, Nano Lett. **16**, 1387 (2016).

[10] V. E. Calado, S. Goswami, G. Nanda, M. Diez, A. R. Akhmerov, K. Watanabe, T. Taniguchi, T. M. Klapwijk, and L. M. K. Vandersypen, Ballistic Josephson junctions in edge-contacted graphene, Nat. Nanotechnol. **10**, 761 (2015).

[11] R. Haller, G. Fülöp, D. Indolese, J. Ridderbos, R. Kraft, L. Y. Cheung, J. H. Ungerer, K. Watanabe, T. Taniguchi, D. Beckmann *et al.*, Phase-dependent microwave response of a graphene Josephson junction, Phys. Rev. Res. **4**, 013198 (2022).

[12] G. Butseraen, A. Ranadive, N. Aparicio, K. R. Amin, A. Juyal, M. Esposito, K. Watanabe, T. Taniguchi, N. Roch, F. Lefloch *et al.*, A gate-tunable graphene Josephson parametric amplifier, Nat. Nanotechnol. **17**, 1153 (2022).

[13] P. Schmidt, L. Banszerus, B. Frohn, S. Blien, K. Watanabe, T. Taniguchi, A. K. Hüttel, B. Beschoten, F. Hassler, and C. Stampfer, Tuning the supercurrent distribution in parallel ballistic graphene Josephson junctions, Phys. Rev. Appl. **20**, 054049 (2023).

[14] J. I.-J. Wang, D. Rodan-Legrain, L. Bretheau, D. L. Campbell, B. Kannan, D. Kim, M. Kjaergaard, P. Krantz, G. O. Samach, F. Yan *et al.*, Coherent control of a hybrid superconducting circuit made with graphene-based van der Waals heterostructures, Nat. Nanotechnol. **14**, 120 (2019).

[15] J. G. Kroll, W. Uilhoorn, K. L. van der Enden, D. de Jong, K. Watanabe, T. Taniguchi, S. Goswami, M. C. Cassidy, and L. P. Kouwenhoven, Magnetic field compatible circuit quantum electrodynamics with graphene Josephson junctions, Nat. Commun. **9**, 4615 (2018).

[16] F. Peñaranda, R. Aguado, E. Prada, and P. San-Jose, Majorana bound states in encapsulated bilayer graphene, SciPost Phys. **14**, 075 (2023).

[17] A. Stern, Non-Abelian states of matter, Nature (London) **464**, 187 (2010).

[18] M. Sato and S. Fujimoto, Majorana fermions and topology in superconductors, J. Phys. Soc. Jpn. **85**, 072001 (2016).

[19] C. Nayak, S. H. Simon, A. Stern, M. Freedman, and S. Das Sarma, Non-Abelian anyons and topological quantum computation, Rev. Mod. Phys. **80**, 1083 (2008).

[20] M. Leijnse and K. Flensberg, Introduction to topological superconductivity and Majorana fermions, Semicond. Sci. Technol. **27**, 124003 (2012).

[21] C. T. Ke, I. V. Borzenets, A. W. Draelos, F. Amet, Y. Bomze, G. Jones, M. Craciun, S. Russo, M. Yamamoto, S. Tarucha *et al.*, Critical current scaling in long diffusive graphene-based Josephson junctions, Nano Lett. **16**, 4788 (2016).

[22] I. V. Borzenets, F. Amet, C. T. Ke, A. W. Draelos, M. T. Wei, A. Seredinski, K. Watanabe, T. Taniguchi, Y. Bomze, M. Yamamoto *et al.*, Ballistic graphene Josephson junctions from the short to the long junction regimes, Phys. Rev. Lett. **117**, 237002 (2016).

[23] X. Du, I. Skachko, and E. Y. Andrei, Josephson current and multiple Andreev reflections in graphene SNS junctions, Phys. Rev. B **77**, 184507 (2008).

[24] C. Ojeda-Aristizabal, M. Ferrier, S. Guéron, and H. Bouchiat, Tuning the proximity effect in a superconductor-graphene-superconductor junction, Phys. Rev. B **79**, 165436 (2009).

[25] I. V. Borzenets, U. C. Coskun, S. J. Jones, and G. Finkelstein, Phase diffusion in graphene-based Josephson junctions, Phys. Rev. Lett. **107**, 137005 (2011).

[26] K. Komatsu, C. Li, S. Autier-Laurent, H. Bouchiat, and S. Guéron, Superconducting proximity effect in long superconductor/graphene/superconductor junctions: From specular Andreev reflection at zero field to the quantum Hall regime, Phys. Rev. B **86**, 115412 (2012).

[27] N. Mizuno, B. Nielsen, and X. Du, Ballistic-like supercurrent in suspended graphene Josephson weak links, Nat. Commun. **4**, 2716 (2013).

[28] J.-H. Choi, G.-H. Lee, S. Park, D. Jeong, J.-O. Lee, H.-S. Sim, Y.-J. Doh, and H.-J. Lee, Complete gate control of supercurrent in graphene *p-n* junctions, Nat. Commun. **4**, 2525 (2013).

[29] T. Li, J. Gallop, L. Hao, and E. Romans, Ballistic Josephson junctions based on CVD graphene, Supercond. Sci. Technol. **31**, 045004 (2018).

[30] D. A. Manjarrés, S. Gómez Páez, and W. J. Herrera, Skewness and critical current behavior in a graphene Josephson junction, Phys. Rev. B **101**, 064503 (2020).

[31] G. Nanda, J. L. Aguilera-Servin, P. Rakyta, A. Kormányos, R. Kleiner, D. Koelle, K. Watanabe, T. Taniguchi, L. M. K. Vandersypen, and S. Goswami, Current-phase relation of ballistic graphene Josephson junctions, Nano Lett. **17**, 3396 (2017).

[32] C. D. English, D. R. Hamilton, C. Chialvo, I. C. Moraru, N. Mason, and D. J. Van Harlingen, Observation of nonsinusoidal current-phase relation in graphene Josephson junctions, Phys. Rev. B **94**, 115435 (2016).

[33] G.-H. Lee and H.-J. Lee, Proximity coupling in superconductor-graphene heterostructures, Rep. Prog. Phys. **81**, 056502 (2018).

[34] G.-H. Park, K. Watanabe, T. Taniguchi, G.-H. Lee, and H.-J. Lee, Engineering crossed Andreev reflection in double-bilayer graphene, Nano Lett. **19**, 9002 (2019).

[35] P. Rickhaus, M. Weiss, L. Marot, and C. Schönenberger, Quantum Hall effect in graphene with superconducting electrodes, Nano Lett. **12**, 1942 (2012).

[36] A. W. Draelos, M. T. Wei, A. Seredinski, C. T. Ke, Y. Mehta, R. Chamberlain, K. Watanabe, T. Taniguchi, M. Yamamoto, S. Tarucha *et al.*, Investigation of supercurrent in the quantum Hall

regime in graphene Josephson junctions, J. Low Temp. Phys. **191**, 288 (2018).

[37] L. Zhao, E. G. Arnault, A. Bondarev, A. Seredinski, T. F. Q. Larson, A. W. Draelos, H. Li, K. Watanabe, T. Taniguchi, F. Amet *et al.*, Interference of chiral Andreev edge states, Nat. Phys. **16**, 862 (2020).

[38] Ö. Gül, Y. Ronen, S. Y. Lee, H. Shapourian, J. Zauberman, Y. H. Lee, K. Watanabe, T. Taniguchi, A. Vishwanath, A. Yacoby *et al.*, Andreev reflection in the fractional quantum Hall state, Phys. Rev. X **12**, 021057 (2022).

[39] M. J. Zhu, A. V. Kretinin, M. D. Thompson, D. A. Bandurin, S. Hu, G. L. Yu, J. Birkbeck, A. Mishchenko, I. J. Vera-Marun, K. Watanabe *et al.*, Edge currents shunt the insulating bulk in gapped graphene, Nat. Commun. **8**, 14552 (2017).

[40] M. T. Allen, O. Shtanko, I. C. Fulga, A. R. Akhmerov, K. Watanabe, T. Taniguchi, P. Jarillo-Herrero, L. S. Levitov, and A. Yacoby, Spatially resolved edge currents and guided-wave electronic states in graphene, Nat. Phys. **12**, 128 (2016).

[41] M. T. Allen, O. Shtanko, I. C. Fulga, J. I.-J. Wang, D. Nurgaliev, K. Watanabe, T. Taniguchi, A. R. Akhmerov, P. Jarillo-Herrero, L. S. Levitov *et al.*, Observation of electron coherence and Fabry-Perot standing waves at a graphene edge, Nano Lett. **17**, 7380 (2017).

[42] J. Ying, J. He, G. Yang, M. Liu, Z. Lyu, X. Zhang, H. Liu, K. Zhao, R. Jiang, Z. Ji *et al.*, Magnitude and spatial distribution control of the supercurrent in Bi_2O_2Se-based Josephson junction, Nano Lett. **20**, 2569 (2020).

[43] P. Rout, N. Papadopoulos, F. Peñaranda, K. Watanabe, T. Taniguchi, E. Prada, P. San-Jose, and S. Goswami, Supercurrent mediated by helical edge modes in bilayer graphene, Nat. Commun. **15**, 856 (2024).

[44] M. Kharitonov, Phase diagram for the $\nu = 0$ quantum Hall state in monolayer graphene, Phys. Rev. B **85**, 155439 (2012).

[45] P. San-Jose, J. L. Lado, R. Aguado, F. Guinea, and J. Fernández-Rossier, Majorana zero modes in graphene, Phys. Rev. X **5**, 041042 (2015).

[46] Y.-M. Xie, É. Lantagne-Hurtubise, A. F. Young, S. Nadj-Perge, and J. Alicea, Gate-defined topological Josephson junctions in Bernal bilayer graphene, Phys. Rev. Lett. **131**, 146601 (2023).

[47] J.-L. Uslu, T. Ouaj, D. Tebbe, A. Nekrasov, J. H. Bertram, M. Schütte, K. Watanabe, T. Taniguchi, B. Beschoten, L. Waldecker *et al.*, An open-source robust machine learning platform for real-time detection and classification of 2D material flakes, Mach. Learn.: Sci. Technol. **5**, 015027 (2024).

[48] See Supplemental Material at http://link.aps.org/supplemental/10.1103/PhysRevB.111.245301 for details on sample fabrication, experimental setup, Fraunhofer-type interference pattern, damping and quality factor, additional Shapiro step measurements, and an extended analysis of the in-plane magnetic field interference pattern.

[49] W. C. Stewart, Current-voltage characteristic of Josephson junctions, Appl. Phys. Lett. **12**, 277 (1968).

[50] D. E. McCumber, Effect of AC impedance on DC voltage-current characteristics of superconductor weak-link junctions, J. Appl. Phys. **39**, 3113 (1968).

[51] S. Shapiro, Josephson currents in superconducting tunneling: The effect of microwaves and other observations, Phys. Rev. Lett. **11**, 80 (1963).

[52] M. Tinkham, *Introduction to Superconductivity*, Dover Books on Physics Series (Dover Publications, Mineola, 2004).

[53] T. F. Q. Larson, L. Zhao, E. G. Arnault, M.-T. Wei, A. Seredinski, H. Li, K. Watanabe, T. Taniguchi, F. Amet, and G. Finkelstein, Zero crossing steps and anomalous Shapiro maps in graphene Josephson junctions, Nano Lett. **20**, 6998 (2020).

[54] S. S. Kalantre, F. Yu, M. T. Wei, K. Watanabe, T. Taniguchi, M. Hernandez-Rivera, F. Amet, and J. R. Williams, Anomalous phase dynamics of driven graphene Josephson junctions, Phys. Rev. Res. **2**, 023093 (2020).

[55] H. Vignaud, D. Perconte, W. Yang, B. Kousar, E. Wagner, F. Gay, K. Watanabe, T. Taniguchi, H. Courtois, Z. Han *et al.*, Evidence for chiral supercurrent in quantum Hall Josephson junctions, Nature (London) **624**, 545 (2023).

[56] Z. Huang, B. H. Elfeky, T. Taniguchi, K. Watanabe, J. Shabani, and D. Shahrjerdi, Observation of half-integer Shapiro steps in graphene Josephson junctions, Appl. Phys. Lett. **122**, 262601 (2023).

[57] G.-H. Lee, S. Kim, S.-H. Jhi, and H.-J. Lee, Ultimately short ballistic vertical graphene Josephson junctions, Nat. Commun. **6**, 6181 (2015).

[58] J. M. Rowell, Magnetic field dependence of the Josephson tunnel current, Phys. Rev. Lett. **11**, 200 (1963).

[59] A. I. Gubin, K. S. Il'in, S. A. Vitusevich, M. Siegel, and N. Klein, Dependence of magnetic penetration depth on the thickness of superconducting Nb thin films, Phys. Rev. B **72**, 064503 (2005).

[60] T. Dvir, A. Zalic, E. H. Fyhn, M. Amundsen, T. Taniguchi, K. Watanabe, J. Linder, and H. Steinberg, Planar graphene-$NbSe_2$ Josephson junctions in a parallel magnetic field, Phys. Rev. B **103**, 115401 (2021).

[61] E. H. Fyhn, M. Amundsen, A. Zalic, T. Dvir, H. Steinberg, and J. Linder, Combined Zeeman and orbital effect on the Josephson effect in rippled graphene, Phys. Rev. B **102**, 024510 (2020).

[62] H. J. Suominen, J. Danon, M. Kjaergaard, K. Flensberg, J. Shabani, C. J. Palmstrøm, F. Nichele, and C. M. Marcus, Anomalous Fraunhofer interference in epitaxial superconductor-semiconductor Josephson junctions, Phys. Rev. B **95**, 035307 (2017).

[63] K. Zuo, V. Mourik, D. B. Szombati, B. Nijholt, D. J. van Woerkom, A. Geresdi, J. Chen, V. P. Ostroukh, A. R. Akhmerov, S. R. Plissard *et al.*, Supercurrent interference in few-mode nanowire Josephson junctions, Phys. Rev. Lett. **119**, 187704 (2017).

[64] S. Hart, H. Ren, M. Kosowsky, G. Ben-Shach, P. Leubner, C. Brüne, H. Buhmann, L. W. Molenkamp, B. I. Halperin, and A. Yacoby, Controlled finite momentum pairing and spatially varying order parameter in proximitized HgTe quantum wells, Nat. Phys. **13**, 87 (2017).

[65] C. Li, B. de Ronde, J. de Boer, J. Ridderbos, F. Zwanenburg, Y. Huang, A. Golubov, and A. Brinkman, Zeeman-effect-induced 0-π transitions in ballistic Dirac semimetal Josephson junctions, Phys. Rev. Lett. **123**, 026802 (2019).

[66] H. Sickinger, A. Lipman, M. Weides, R. G. Mints, H. Kohlstedt, D. Koelle, R. Kleiner, and E. Goldobin, Experimental evidence of a φ Josephson junction, Phys. Rev. Lett. **109**, 107002 (2012).

[67] D. B. Szombati, S. Nadj-Perge, D. Car, S. R. Plissard, E. P. A. M. Bakkers, and L. P. Kouwenhoven, Josephson ϕ_0-junction in nanowire quantum dots, Nat. Phys. **12**, 568 (2016).

[68] W. Albrecht, J. Moers, and B. Hermanns, HNF—Helmholtz Nano Facility, J. Large Scale Res. Facil. JLSRF **3**, A112 (2017).

[69] https://doi.org/10.5281/zenodo.14639763.